Brief Report

Shock-Discharge Interaction Model Extended into the Third Dimension

Anna Markhotok *

Posted Date: 22 January 2024

doi: 10.20944/preprints202401.1581.v1

Keywords: Hypersonic Plasma Dynamics; Shock Wave Refraction; Shock-Plasma Interaction

 doi:10.20944/preprints202401.1581.v1

Brief Report

Shock-Discharge Interaction Model Extended into the Third Dimension

A. Markhotok

Physics Department, Old Dominion University, Norfolk, VA 23529 USA;
amarhotk@phys.washington.edu

Abstract: This work is an addition to the previously developed two-dimensional model of the shock-plasma interaction extending it into the third dimension. The model allows tracing the evolution of the state of the hypersonic flow and the shock front refracted at a thermal discontinuity. The advantages of using the spherical coordinate system for this type of the problems include more transparency in interpreting the solution and a shortened calculation procedure, because all the changes to the front become reduced to one distortion component only. Although the vorticity generation triggered at the interface is the consequence of the refraction and tied to the steep changes of the front, it is shown here that it is not because of an instant parameter jump at the interface due to refraction itself.

Keywords: hypersonic plasma dynamics; shock wave refraction; shock-plasma interaction

I. Introduction

The previously developed two-dimensional model [1] describes the state of the shock front and the changes to the hypersonic flow behind it as a result of interaction with a thermal discontinuity created in a discharge, a flame, or an interstellar environment. [2,3]. This work is a short addition to the model extending it into the third dimension. Both open and closed interfaces of an arbitrary shape are covered by the existing model in the plane of symmetry oriented along the shock propagation direction that corresponds to the cylindrical symmetry case. In describing the evolution of the hypersonic flow with time, the model essentially relates the perturbation to the front with the incident shock, plasma medium, and the interface geometrical parameters. Under definite conditions, the dynamics of the perturbation to the front represents an instability that develops in the form of wave-like stretchings into the lower density medium followed with the loss of stability in the flow behind it, that eventually evolves into an intense vortex structure. The instability mode in this case is aperiodical and unconditional, and the shock state evolves with either a transition to another stable state or continuous development as a secondary flow [4]. The instability features a set of interesting features, such as: a similarity law in the spatial and temporal evolution of the perturbations with respect to the interface curvature; the instability locus independence of the gas density distribution thus identifying the interface conditions as the sole triggering factor; the specific role of the density gradient in the instability evolution discriminating between qualitatively different outcomes; the possibility of decay via non-viscous dumping mechanisms; and the connection between the shock and the interface stability.

Both a sharp and an extended type of the interface can be accommodated within the model, resulting in considerable difference in the refraction effect [5]. If accounting for real-gas effects, the model predicts significant deviations in the shock reflection and refraction strengths at the interface with plasma [6], and shows that the presence of thermodynamic non-equilibrium in the hypersonic flow can result in variation of the shock wave structure during the interface crossing and interaction with plasma medium [7]. Studying the dynamics for the two components of the front distortion in the longitudinal and transversal directions revealed another interesting feature of the interaction

 doi:10.20944/preprints202401.1581.v1

showing the possibility of vorticity generation in the hypersonic flow behind the refracted front. It is triggered at the interface due to parameter re-distribution in the flow behind the front and continues inside the plasma spot in an intense non-linear dynamics mode [1]. The induced rotation of the shock velocity components tended to occur under definite conditions and typically attributed to the front portion undergoing the most steep changes. In this connection, considering the model in 3*D* would allow one to see whether the presence of the third dimension in the interaction can instantly produce a component of the shock velocity at the interface due to refraction itself, resulting in an additional spinning of the front elements around the longitudinal symmetry axis.

In the following examples, two problems featuring the spherical and cylindrical geometries will be solved numerically in 3*D* and the results for the front profiles will be matched to those obtained with the 2*D* model.

II. Refraction parameters and the shock distortion components in 3*D*

The aim of this paragraph is determining the shock refraction parameters and the front distortion in 3*D* with time as a function of the interface coordinates. It will be assumed that the plasma medium inside the sphere is heated to the temperature T_2, and the gas surrounding the sphere is kept at T_1 and the same pressure $p_1 = p_2 = p_{atm}$. A planar shock wave will be incident on a spherical interface in the x-direction with the velocity V_1, as shown in Figure 1, i.e.

$$\overrightarrow{V_1} = V_{1x}\hat{x} \tag{1}$$

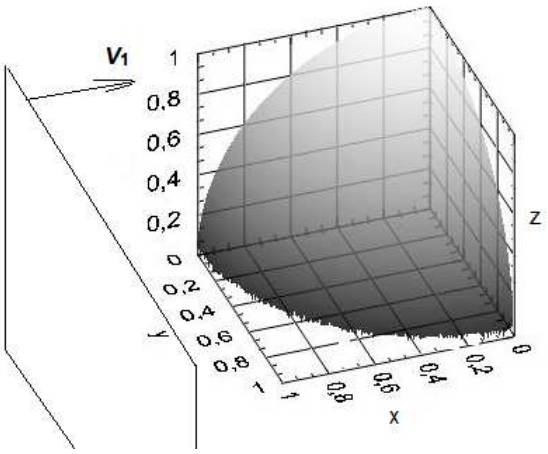

Figure 1. Schematic diagram of a planar shock wave incident on a spherically shaped heated spot with a velocity V_1 along the x-direction.

In the spherical coordinate system this translates into a three-component vector

$$\overrightarrow{V_1} = V_{1x}\left(sin(\theta)cos(\varphi)\hat{r} + cos(\theta)cos(\varphi)\hat{\theta} - sin(\varphi)\hat{\phi}\right) \tag{2}$$

where (x,y,z) and (r,θ,φ) are the corresponding coordinates of the point of interaction (i) on the sphere, θ is the angle between the r- and z-directions, the angle φ is in the x-y plane, the symbol "hat" over a coordinate denotes the unit vector in the corresponding direction,
and the angles φ and θ are determined as

$$\theta = tan^{-1}\left(\sqrt{x^2 + y^2}/z\right), \;\; \varphi = tan^{-1}(y/z) \tag{3}$$

The component of the velocity normal to the surface, which its the radial component,

$$V_{1r} = V_{1n} = V_{1x}sin(\theta)cos(\varphi) \tag{4}$$

and the tangential component

$$\overrightarrow{V_{1\tau}} = V_{1x}\left[cos(\theta)cos(\varphi)\hat{\theta} - sin(\varphi)\hat{\phi}\right] \tag{5}$$

Preprints.org (www.preprints.org) | NOT PEER-REVIEWED | Posted: 22 January 2024 doi:10.20944/preprints202401.1581.v1

Then the incidence angle α defined as the angle between vector V_1 and the normal to the sphere at the point (i), is determined by the relation

$$cos(\alpha) = sin(\theta)cos(\varphi) \tag{6}$$

The velocity V_2 of the shock wave refracted into the hot sphere is obtained through its normal and tangential components, V_{2n} and $V_{2\tau}$. The normal component of the velocity V_{2n} is determined by the ratio of normal components of the Mach number $M_{2n}(M_{1n})$ that is obtained from a pair of shock refraction equations, depending on the temperature ratio condition across the interface [6],

$$V_{2n} = \epsilon V_{1n}, \qquad \epsilon = M_{21}^{(n)}\sqrt{T_{21}} \tag{7}$$

where $T_{21} = T_2/T_1$ and $M_{21}^{(n)} = M_{2n}/M_{1n}$,
from which

$$V_{2n} = \epsilon V_{1x} sin(\theta)cos(\varphi) \quad , \; V_{1x} = V_1 \tag{8}$$

Using the continuity principle for tangential components across the interface,

$$V_{2\tau} = V_{1\tau} \tag{9}$$

the shock velocity vector inside the sphere for the front element crossed the point (I) takes the form

$$\overrightarrow{V_2} = V_{1x}\left(\epsilon sin(\theta)cos(\varphi)\hat{r} + cos(\theta)cos(\varphi)\hat{\theta} - sin(\varphi)\hat{\phi}\right), \tag{10}$$

Then the refraction angle γ, as the one between vectors V_1 and V_2, is determined by the following equation

$$cos\gamma = \frac{cos^2\varphi(\varepsilon sin^2\theta + cos^2\theta) + sin^2\varphi}{\sqrt{cos^2\varphi(\varepsilon^2 sin^2\theta + cos^2\theta) + sin^2\varphi}} \tag{11}$$

In the next step, the shock front distortion can be found by following a path of a small element "s" of the incident shock front through the plasma inside the sphere, as shown in Figure 2.

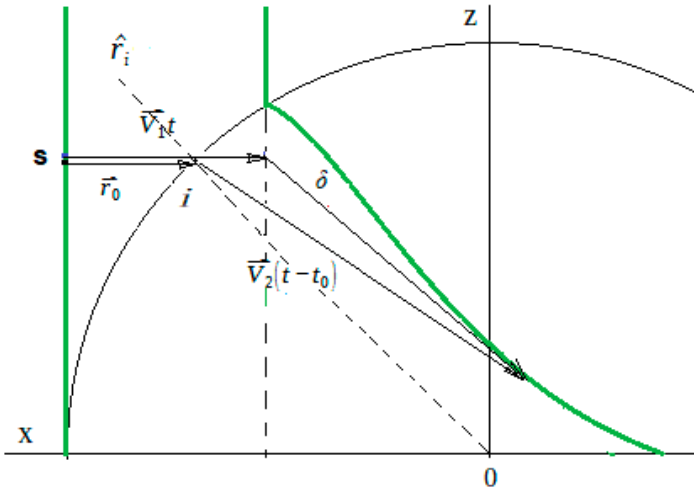

Figure 2. The initially planar shock front (green vertical line) distorted (green curve) during its refraction into a spherical plasma spot, projected into the (z,x)-plane.

In the reference frame moving with the velocity V_1, the distortion vector

$$\vec{\delta} = \vec{r_0} + \overrightarrow{V_2}(t - t_0) - \overrightarrow{V_1}t \tag{12}$$

where t is the interaction time starting at the moment the initially planar shock arrives at the location $x = R$, R is the sphere radius, r_s is the radial coordinate of the small element "s" that is eventually crossing the sphere at the interaction point "i", $\vec{r_0} = \vec{r_s} - \vec{r_i}$is the local displacement for the time t_0 of

 doi:10.20944/preprints202401.1581.v1

the shock's approaching the interface, and the third term in the righthand side of eq. (12) is introduced to obtain the front coordinates relative to the portion of the front undisturbed by the plasma spot.

For the shock front approaching the interface along the x-direction,

$$\overrightarrow{r_0} = (R - x_i)\left[sin(\theta)cos(\varphi)\hat{r} + cos(\theta)cos(\varphi)\hat{\theta} - sin(\varphi)\hat{\phi}\right] \tag{13}$$

and, using (3) and (10), the eq. (12) transforms into

$$\begin{aligned}\vec{\delta} = \hat{r}sin(\theta)cos(\varphi)[(R - x_i) + \varepsilon V_1(t - t_0) - V_1 t] + \hat{\theta}cos(\theta)cos(\varphi)[(R - x_i) - V_1 t_0] \\ - \hat{\phi}sin(\varphi)[(R - x_i) - V_1 t_0]\end{aligned} \tag{14}$$

where the angles φ and θ are referred to the point of interaction i.

Since $t_0 = (R - x_i)/V_1$, the $\hat{\theta}$- and $\hat{\phi}$-components of the distortion in eq. (14) are equal to zero,

$$\overrightarrow{\delta_\theta} = \overrightarrow{\delta_\varphi} = 0 \tag{15}$$

and the expression (14) takes the final form

$$\vec{\delta} = \overrightarrow{\delta_r} = \hat{r}sin(\theta)cos(\varphi)(\varepsilon - 1)[V_1 t - (R - x_i)], t > t_0 \tag{16}$$

from which it immediately follows that all the changes in the front occur in the radial direction only. It should be noted that the "radial" direction has a current status as it is dependent on the position of the interaction point "i", and thus it changes as the interaction point progresses along the interface surface, starting from being in the (x,y)-plane at {$t = 0$, $x = R$} until it ends up in the (z,y)-plane (at $x = 0$). Consequently, referring to Figure 2, the vector δ_r will always be parallel to the current radial direction r_i drawn through the interaction point i.

Going back to the cartesian coordinate system, to determine the projections of eq. (16) onto the (x, y, z)-basis, the factor ε in (7) should be first expressed in the spherical coordinate system. In accordance to the the results in [6], the normal component of the Mach number $M_2^{(n)}$ is a function of M_{1n} that is very close to linear,

$$M_{2n} = \zeta + \eta M_{1n} = f(M_{1n}) \tag{17}$$

where the factors ζ and η are numerical coefficients that are dependent on the Mach number M_1, the ratio T_{21}. and the specific heat ratio constants for the two media.
Then, with

$$M_{1n} = M_1 sin(\theta)cos(\varphi) \tag{18}$$

and eqs.(4, 7), we obtain

$$\epsilon = \sqrt{T_{21}}\,[\zeta + \eta M_1 sin(\theta)cos(\varphi)]/M_1\, sin(\theta)cos(\varphi) \tag{19}$$

from which, and in accordance to eq. (16),

$$\delta_r = sin(\theta)cos(\varphi)\left\{\sqrt{T_{21}}\,[\zeta + \eta M_1 sin(\theta)cos(\varphi)]/[M_1 sin(\theta)cos(\varphi)] - 1\right\}[V_1 t - (r_s - R)] \tag{20}$$

and the three cartesian components of the distortion are

$$\delta_x = \delta_r sin(\theta)cos(\varphi), \quad \delta_y = \delta_r sin(\theta)sin(\varphi), \quad \delta_z = \delta_r cos(\theta) \tag{21}$$

The eq.(20) can be more generalized by presenting it in a dimensionless form if scaling δ_r with the characteristic length R and time – with $\tau = R/V_1$. Then, for the dimensionless time $\bar{t} = t/\tau$ and the coordinates $\bar{\delta} = \delta/R$, $\bar{r_s} = r_s/R$, it yields the following dimensionless equation for δ_r

$$\bar{\delta}_r = sin(\theta)cos(\varphi)\left\{\sqrt{T_{21}}\,[\zeta + \eta M_1 sin(\theta)cos(\varphi)]/[M_1 sin(\theta)cos(\varphi)] - 1\right\}[\bar{t} - (\bar{r_s} - 1)] \tag{22}$$

and its cartesian components correspondingly

$$\bar{\delta}_x = \bar{\delta}_r sin(\theta)cos(\varphi), \quad \bar{\delta}_y = \bar{\delta}_r sin(\theta)sin(\varphi), \quad \bar{\delta}_z = \bar{\delta}_r cos(\theta), \tag{23}$$

where the "bar" over a variable means its dimensionless equivalent.

 doi:10.20944/preprints202401.1581.v1

III. Numerical results for a spherical and cylindrical geometries

For illustration purposes and for matching with the 2*D* model results (in the two planes of symmetry), a numerical simulation was done for a particular case of non-dissociating nitrogen gas heated to temperature $T_2 = 2000\ K$ and the outside temperature of $T_1 = 300\ K$, the incident shock Mach number $M_1 = 3.5$, and $p = p_{atm}$. In the slow-fast scenario present at the entrance of the heated spot, the ratio of normal components of the Mach number in (7) is obtained using the refraction equation that assumes that the reflected wave is a rarefaction wave. For the shock and gas conditions considered here, the function $M_{2n} = f(M_{1n})$ has been already determined in [6] and the factors ζ and η in (17) can be borrowed from there. With those parameters in place, the radial component of the front distortion δ_r, and its projections into the Cartesian basis δ_x, δ_y, δ_x are calculated using eqs. (20,21). The simulation results in the (z,y)-plane, that is transversal to the shock incidence direction, are presented in Figure 3 and correspond to the dimensionless time $n_t = 1.0$.

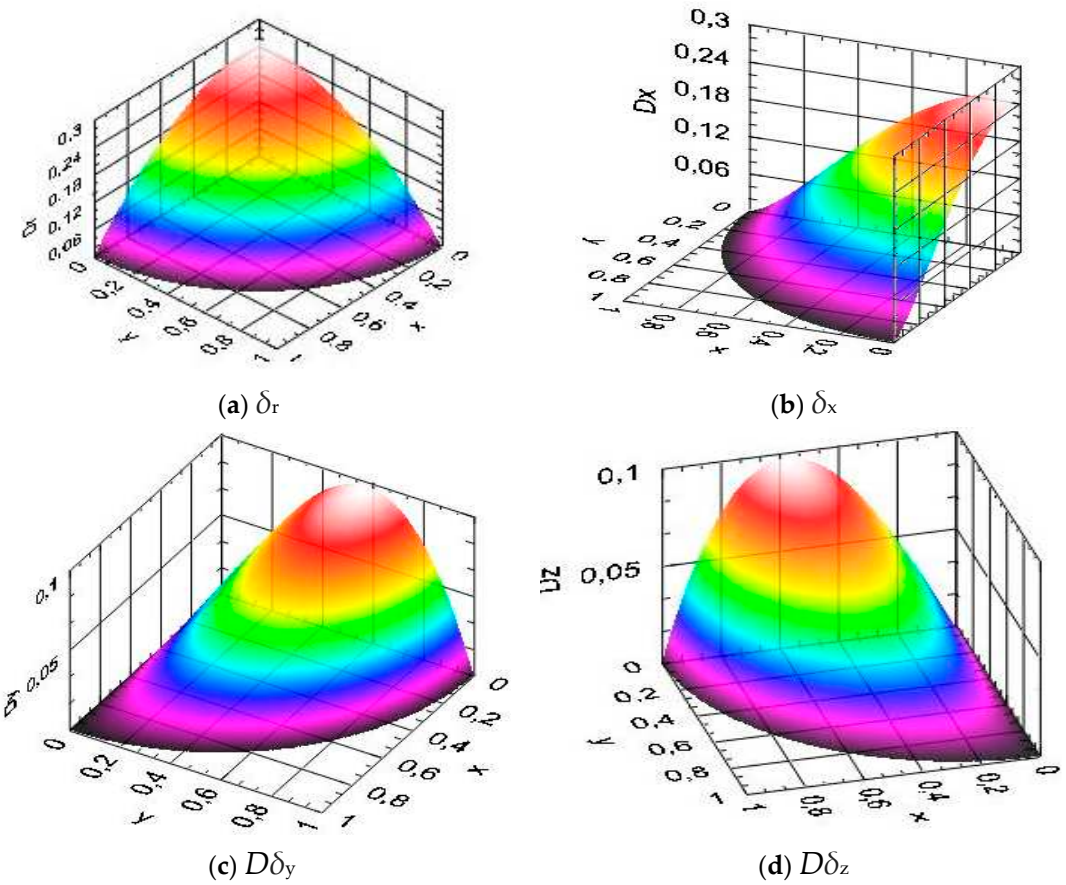

(**a**) δ_r (**b**) δ_x

(**c**) $D\delta_y$ (**d**) $D\delta_z$

Figure 3. The distortion components δ_r, δ_x, δ_y, and δ_z at the moment of time $n_t = 1.0$, plotted in the (z,y)-plane. Diatomic nitrogen gas at $T_1 = 300\ K$, $T_2 = 2000\ K$, $M_1 = 3.5$, and $p = p_{atm}$.

In the longitudinally oriented (x,y)-plane, the results are presented in Figure 4.

Preprints.org (www.preprints.org) | NOT PEER-REVIEWED | Posted: 22 January 2024 doi:10.20944/preprints202401.1581.v1

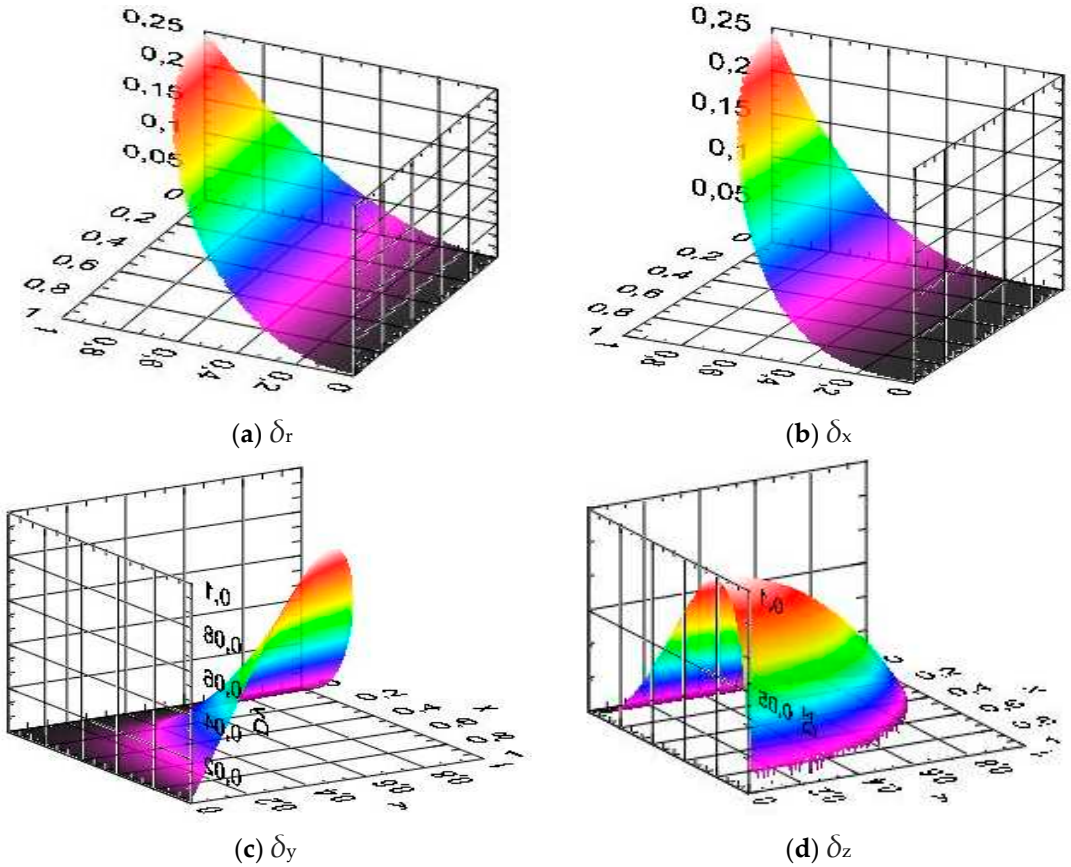

(**a**) δ_r (**b**) δ_x

(**c**) δ_y (**d**) δ_z

Figure 4. The distortion components δ_r, δ_x, δ_y, and δ_z at the moment of time n_t = 1.0, plotted in the (x,y)-plane, for the same shock and gas parameters as in Figure 3.

As the plots in Figure 3 demonstrate, the distributions for δ_r and δ_x, in the radial and longitudinal directions are fully symmetrical, as well as those in Figure 4, exhibiting the same tendency and maximum locations. Projecting the profiles into the two planes of symmetry in Figures 3 and 4, it can be seen that they are similar to those obtained with the 2D model in [8] (Figure 5). In the plot of Figure 5, the curve used for comparison at the moment of time n_t = 1.0 is the one crossing the sphere pole.

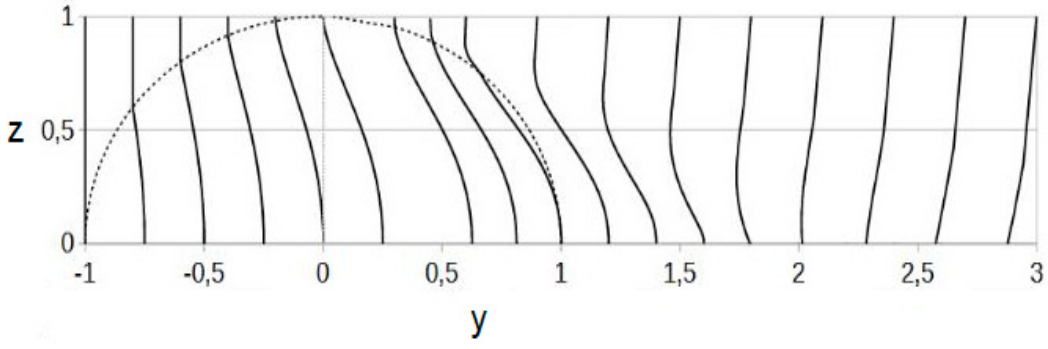

Figure 5. Shock profiles obtained with 2D model in the (z,y)-plane at various times, for the same shock and gas parameters as in the Figure 3. The curve crossing the sphere pole correspond to the time n_τ = 1.0.

Comparing the data in the Figures 3, 4 and Figure 5 quantitatively, it is seen that maximum distortion δ_x = 0.25 taking place at the longitudinal symmetry axis coincides with that value and location in Figure s 3 and 4. Thus, in both planes of symmetry, the 3D model transitions exactly into its 2D equivalent (φ = 0).

 doi:10.20944/preprints202401.1581.v1

A problem featuring the cylindrical symmetry can be considered here using the polar coordinate system (i.e. what the 2*D* model is applied to), in which the derived above relations are reduced to the planar case by taking $\varphi = 0$ and leaving θ as a variable, resulting in $y_i = 0$, $y_s = 0$, and $\delta_y = 0$. In this case the problem corresponds to a planar shock interacting with an interface of a cylindrical shape that is shown with the gray-colored surface in Figure 6a. The results for the distortion profiles at the time $n_t = 1.0$ and the same shock and gas parameters as above, are presented in the Figure 6, b-c.

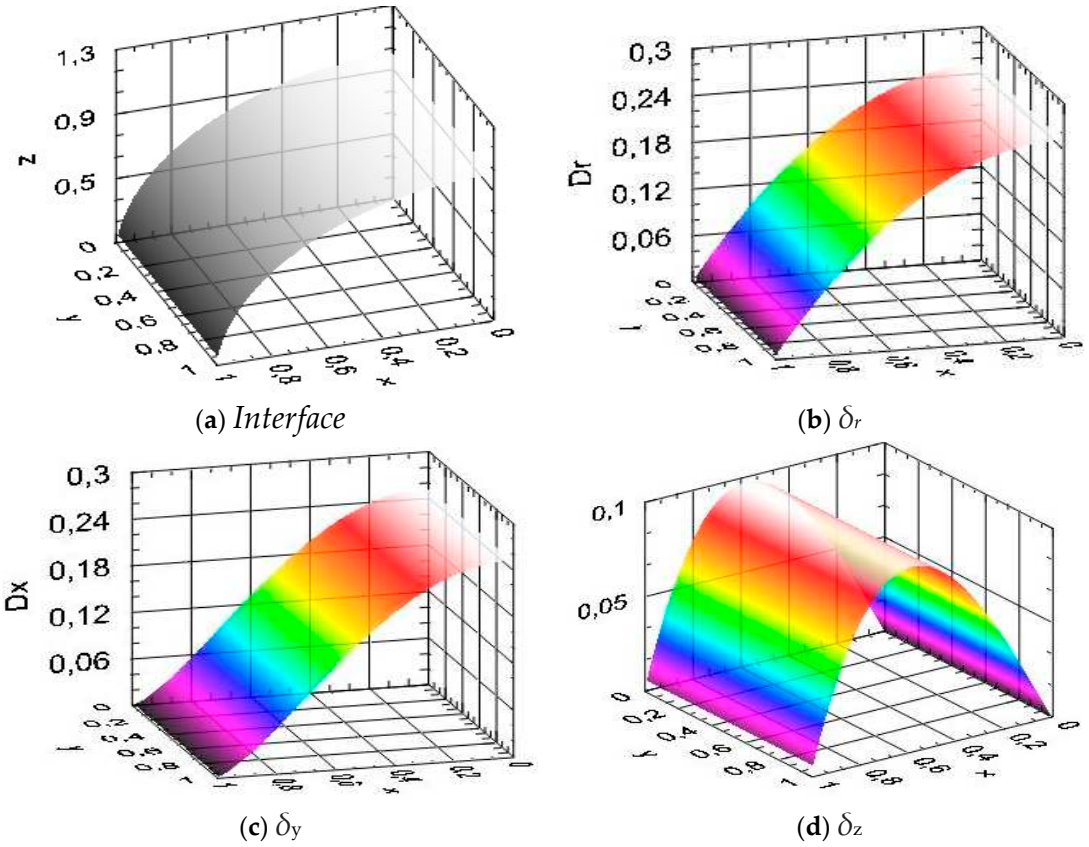

(**a**) *Interface* (**b**) δ_r

(**c**) δ_y (**d**) δ_z

Figure 6. The initially planar shock front modification in the case of cylindrical symmetry, at the time $n_t = 1.0$ and the same shock and gas parameters as in the Figure 3.

The profiles are matching those in the previous figures when projected into the planes of symmetry, as well as those in Figure 5, if taken as a slice in the (z,x)-plane. The results for the two models match analytically as well, if different definition of the angles are accounted for using the transition $\theta \rightarrow \pi/2 - \alpha$.

VII. Conclusion

The examples based on the 3D spherical coordinate representation illustrated that the front distortion in the transversal plane exhibit fully symmetrical distribution, thus obviously validating the use of the 2D model in spherically symmetrical problems as well. The projection of the 3*D* results on the two planes of symmetry coincide with those obtained with 2*D* model, thus making the 3*D* model relations exactly transitioning into its 2*D* equivalent (at $\varphi = 0$).

Considering the interaction problem in 3*D* showed that it is advantageous using the spherical coordinate system over cartesian as all the changes to the front become reduced to one component of the distortion vector only. This is the direct consequence of the continuity principle for the tangential components of the velocity, from which it follows that there will be no change in the distortion vector components in the azimuthal and orbital directions. It immediately follows then that the zero tangential components of the distortion vector at the interface exclude the possibility of an additional spinning of the front elements due to refraction itself. In relating this result to the phenomena of

vorticity generation triggered at the interface and described in [1], it should be noted the following difference. While there is no instant, jump-like rotation of the shock velocity vector at the moment of refraction at the interface, the positive dynamics in the radial component of the front distortion initiates and further supports the production of vorticity. As it was shown in [1], the vorticity is triggered and amplified at the locations of the most steep changes of the front. Thus presentation of the distortion components in the spherical coordinate system offers a transparent way to show and essentially rule out the possibility of an instant vorticity generation at the interface. It points to the mechanism of a different nature and location referring the vorticity production to later times of the shock propagation rather than at the interface.

As another bonus of the spherical coordinate representation, the form of the solution obtained here becomes more transparent for interpreting. It also significantly shortens the calculation by eliminating a set of parameters needed in the procedure, such as the incident and refraction angles, and associated to this Mach number and velocity components, etc. As in the 2*D* model, the 3*D* relations are presentable in a dimensionless form and thus can be applied to a wider range of applications.

References

1. A. Markhotok, "Wave Drag Modification in the Presence of Discharges", a book chapter in "Compressible flows and shock waves", IntechOpen, September 27, 2019. DOI: http://dx.doi.org/10.5772/intechopen.86858
2. Ya. B. Zeldovich, Yu. P. Raizer, *Physics of Shock waves and High-Temperature Hydrodynamic Phenomena*, Academic Press, New York and London, 1967.
3. D. Bushnell, Shock wave drag reduction, Ann. Rev. Fluid Mech., 2004.36:81-96,2004,
4. DOI: 10.1146/annurev.fluid.36.050802.122110.
5. A. Markhotok, "A shock wave instability induced on a periodically disturbed interface", IEEE Transactions on Plasma Science **46**, Issue 8, pp. 2821 – 2830 (2018), DOI: 10.1109/TPS.2018.2848597.
6. A. Markhotok, S. Popovic, "Refractive phenomena in the shock wave dispersion with variable gradients", J. of Appl. Phys. **107**, 123302, 2010.
7. A. Markhotok, "The Effect of Gas Nonideality on the Interface Reflectivity When Interacting With a Shock Wave," IEEE Transactions on Plasma Science. **48**, Issue 11, Nov. 2020, pgs. 3759-3767. doi: 10.1109/TPS.2020.3026953.
8. A. Markhotok, "Nonequilibrium Factor in the Structure of a Curved Shock Wave Refracted Into an Intensively Heated Medium", IEEE Transactions on Plasma Science, March 2022,V.50, Issue 3, pgs. 596-608, DOI:10.1109/TPS.2022.3147216.
9. A. Markhotok, "Non-symmetry in the Shock Refraction at a Closed Interface as a Recovery Mechanism", Doi: 10.20944/preprints 202311.0902.v1. Submitted to Dynamics Mdpi, 2023.